Change of magnetic property during austenitizing process of Fe-Cr-Ni-Al-C alloy

SHIN-ICHIRO YOKOYAMA
Metallurgical Research Laboratory, Hitachi Metals Ltd., 2107-2 Yasugi-cho Yasugi Shimane, 692-8601, Japan

YORITOSHI MINAMINO
Department of Adaptive Machine Systems, Graduate School of Engineering, Osaka University, 2-1 Yamadaoka, Suita, Osaka, 565-0871, Japan

Published online: 12 January 2006

Effects of austenitization temperatures and holding time on magnetization, *J* (T), of Fe-17.5 mass%Cr-2.0 mass%Ni-0.8 mass%Al-0.5 mass%C based alloy were investigated in order to clarify the heat treatment condition for austenitizing and quantify the relation between magnetic properties and microstructures. The alloy exhibited high *J* value of 1.46 T after annealing at 1053 K. On the other hand, the *J* values of the alloy after austenitizing at temperatures between 1273 and 1473 K lowered with increasing austenitization temperature, describing s-shape curves. The *J* value of the alloy after austenitizing at temperatures above 1423 K for 240 s was nearly equal to zero magnetization. In addition, they also lowered with the increase of the holding time between 1 s and 240 s. The decrease in *J* values by austenitizing was closely related to the dissolution of the $M_{23}C_6$ particles into austenite (γ) matrix phase, which proceeds at higher temperature for longer time. The increase in chromium and carbon concentration in γ matrix phase due to the dissolution of $M_{23}C_6$ particles resulted in the decrease in martensite start (M_s) and finish (M_f) temperatures, and the increase in the paramagnetic retained γ fraction ($X_{\gamma R}$). The following equation was introduced on the relation between magnetization and retained γ fraction.

$$J_\gamma / J_\alpha = 0.49X_{\gamma R}^2 - 1.50X_{\gamma R} + 0.99$$

J_γ means the *J* values of the alloy after austenitizing at temperatures between 1273 and 1473 K, while J_α means that of the alloy after annealing at 1053 K (=1.46T).

1. Introduction

According to the phase diagram, most of iron-based alloys have ferromagnetic ferrite (α) and paramagnetic austenite (γ) phases below the A_1 temperatures and above the A_3 temperatures respectively [1]. Therefore, the heat treatments of these alloys from the temperatures above A_{c3} to lower temperatures can change their phase structures, e.g., the α phase, retained γ phase, pearlite, martensite phase and so on. The selection of alloys and special heat treatments enable us to produce some kinds of iron-based alloys, which have ferromagnetic and paramagnetic properties at ambient temperatures [2–4]. For example, an Fe-17.8 mass%Cr-2.0 mass%Ni-1.0 mass%Al-0.5 mass%C alloy, which has relative maximum permeability of $\mu_m =$ 952, magnetic flux density of B = 1.30(T) at 4000 Am^{-1} and coercive force of H_c = 540 (Am^{-1}) after annealing at 1053 K below the A_{C1} temperature (1085 K), exhibits much lower relative permeability of $\mu_r = 1.02$ after austenitizing at 1473 K above the A_{C3} temperature (1142 K) for 0.6 ks [4].

This alloy is industrially applied to an electric motor component, which has narrow paramagnetic portions in a ferromagnetic body [5]. The narrow paramagnetic portions are produced by the partial austenitizing heat treatment. Therefore, the basic data on the heat treatments for austenitizing the Fe-Cr-Ni-Al-C alloy are practically required in order to clarify the effect of austenitizing conditions on magnetic properties and microstructures. In

0022-2461
DOI: 10.1007/s10853-005-2638-8

addition, the prediction of magnetic property from the microstructure is also required because it is difficult to measure the exact magnetic property of the narrow paramagnetic portions in the actual products. However, studies on the relation between magnetic properties and microstructures during the austenitizing process of Fe-Cr-Ni-Al-C and its similar alloys have not been found. Therefore, the purpose of this study is to clarify the effects of austenitizing temperatures and holding time on magnetization of the Fe-Cr-Ni-Al-C based alloy, and to quantify the correlation between magnetization and microstructures.

2. Experimental procedures

The chemical compositions of two kinds of Fe-17.5 mass%Cr-2.0 mass%Ni-0.8 mass%Al -0.5 mass%C based alloys, with about 0.2 mass% of silicon and 0.5 mass% of Mn as impurities, are listed in Table I. Their chemical compositions are quite similar, but their preparing processes are different. The #1 alloy sheet, with 0.35 mm in thickness, was prepared by mass production; a cold rolling with reduction rate of 65%, following annealing at 1053 K for 180 s in (N_2+8%H_2) gas, and then cooling in the air. This sheet is referred to as "the annealed #1". On the other hand, the #2 ingot was produced using vacuum induction melting, and then homogenized at 1443 K for 36 ks in the air, and slowly cooled in the furnace. The homogenized ingot was hot forged at 1373 K, and the block, with 20×80×400 mm in size, was obtained. The block was annealed at 1053 K for 14.4 ks and then slowly cooled in the air. This annealed block is referred to as "the annealed #2".

The samples with 0.35×4×6 mm (#1) and 1×4×6 mm (#2) in size were cut out from these annealed alloys for the measurement of the magnetization, while the samples with 0.35×10×15 mm (#1) and 1×10×15 mm (#2) in size were also cut out for the observation of the microstructures and the phase analysis. Some of the samples were heat treated for austenitizing at temperatures between 1273 K and 1473 K for 1–240 s in a salt bathing furnace and subsequently cooled in the air. The magnetization, J (T), of #1 and #2 was measured with a vibrating sample magnetometer (VSM) under the exciting magnetic field of μ_0H = 1(T). The microstructures of #1 were observed using a scanning electron microscope (SEM), and the diameter and the volume fraction of carbides in the microstructures were measured by analyzing the SEM images. The phases of #1 were identified by X-ray diffractometry (XRD), but the #1 sheet, with rolled texture, is not suitable for the quantitative measurement of retained austenite fraction, $X_{\gamma R}$, because the isotropic polycrystalline sample, without texture, is required in order to determine the $X_{\gamma R}$ values by XRD [6]. Therefore, #2 was used for the determination of the $X_{\gamma R}$ values. In addition, the samples with ϕ3×10 mm were cut out from the annealed #2, and held at temperatures between 1273 and 1473 K for 240 s in a vacuum chamber, and then subsequently N_2 gas cooled to 123 K. The martensite start (M_s) and finish (M_f) temperatures were determined from the expansion curves in N_2 gas cooling.

TABLE I Chemical compositions of the samples (mass%)

Samples	C	Si	Mn	Ni	Cr	Al	Fe	Note
#1	0.52	0.20	0.48	2.06	17.59	0.77	Bal.	Cold rolled and then annealed
#2	0.50	0.18	0.51	2.02	17.28	0.76	Bal.	Hot forged and then annealed

3. Results and discussion

Fig. 1 shows the austenitization temperature dependences of *J* (T) values, with 1.46 T of the annealed #1 and #2 drawn as a horizontal broken line. The *J* values decrease with increasing austenitization temperatures, describing s-shape curves. The curves of #1 and #2 after 240 s of holding exhibit similar tendencies to each other. Therefore, these two alloys are not distinguished from each other in the following results and discussion. The *J* values are nearly equal to zero magnetization after austenitizing at temperatures above 1423 K for 240 s, but they exhibit higher values when the holding time is shorter. The detailed effects of holding time on *J* values are shown in Fig. 2. The *J* values steeply decrease from that of the annealed one in the beginning at each temperature, and then gradually decrease with holding time. Especially at 1423 K and 1473 K, the *J* values approach zero magnetization in short time. However, the magnetization has the

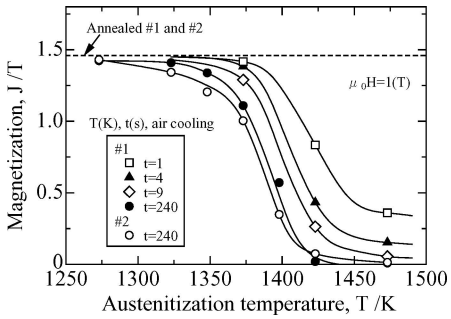

Figure 1 Effects of austenitization temperatures on magnetization.

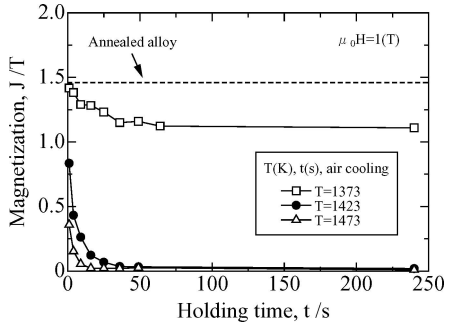

Figure 2 Effects of holding time on magnetization.

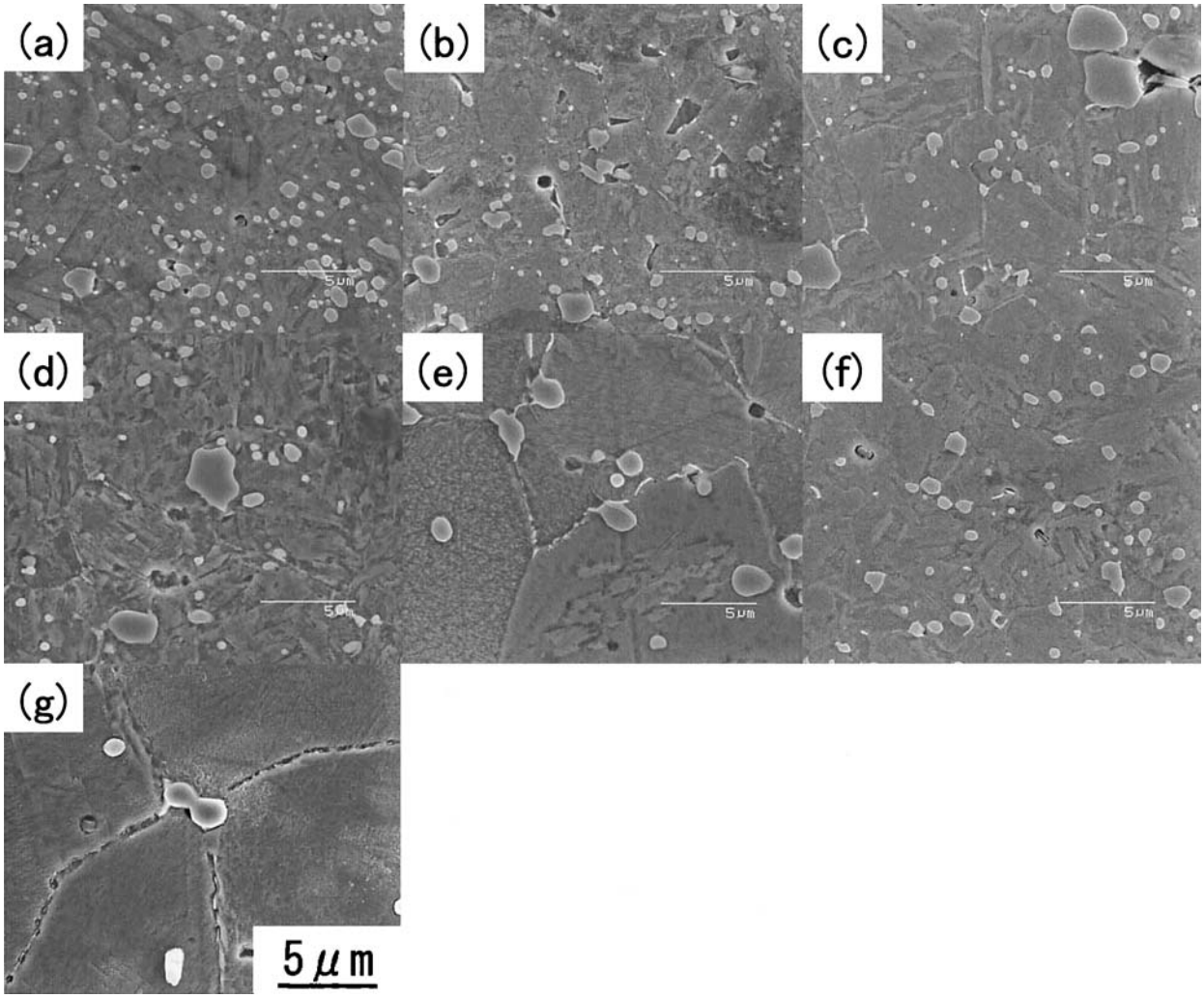

Figure 3. SEM microstructures of the alloy after (a) annealing at 1053 K for 180 s, (b)–(e) austenitizing at 1423 K for (b) 1 s (c) 4 s (d) 9 s (e) 240 s, and (f)–(g) austenitizing at (f) 1373 K and (g) 1473 K for 240 s.

high J value of 1.11 T even at the long holding time of 240 s at 1373 K.

Figs. 3 and 4 respectively show the SEM structures and XRD patterns of (a) annealed and (b)–(g) austenitized alloy. Carbide particles are observed in all SEM images in Fig. 3, and all of them are identified as $M_{23}C_6$ in the XRD patterns in Fig. 4A. The existence of $M_{23}C_6$ is consistent with ternary Fe-Cr-C phase diagrams reported by Kuo at 973 K [7], and by Bungardt *et al*. in the temperature range between 1123 and 1423 K [8]. From Fig. 3a, a lot of spherical $M_{23}C_6$ particles exist in the annealed alloy. The mean diameter of the particles is 0.63μm, and the volume percent of the particles in the structure is 8.3%. On the other hand, the amount of the $M_{23}C_6$ particles observed in the structures after austenitizing at 1423 K for 1, 4, 9 s and 240 s is smaller than that of the annealed structure, and decrease with the proceeding of time as shown in Fig. 3b–e. The volume percent of the $M_{23}C_6$ particles in their structures is 3.4% (1 s), 2.5% (4 s), 2.4% (9 s) and 0.8% (240 s), respectively. It is thought that this decrease in the amount of the $M_{23}C_6$ particles

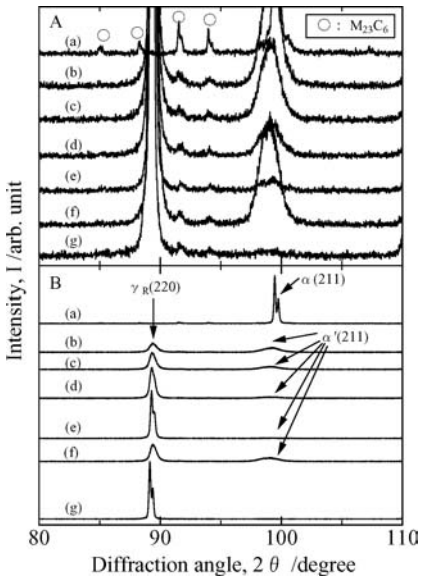

Figure 4 X-ray diffraction patterns of the alloy after (a) annealing at 1053 K for 180 s, (b)–(e) austenitizing at 1423 K for (b) 1 s (c) 4 s (d) 9 s (e) 240 s, and (f)–(g) austenitizing at (f) 1373 K and (g) 1473 K for 240 s.

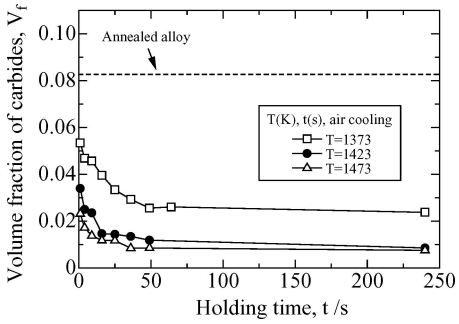

Figure 5 Effects of holding time on volume fraction of carbide particles in the microstructures.

is due to the dissolution of $M_{23}C_6$ into γ matrix phase. Furthermore, the long holding time tends to coarsen the $M_{23}C_6$ particles, and large particles, with about 2.5μm square size, are observed in the structures after 4 and 9 s of holding as shown in Fig. 3c and d, respectively. After 240 s of holding, only spherical $M_{23}C_6$ particles, with 1.29 μm in mean diameter, remain in the structure of Fig. 3e, and the fine particles are not observed there. It is considered that this coarsening of the $M_{23}C_6$ particles with time is due to the Ostwald ripening of the undissolved particles, while the fine ones dissolve into the γ matrix phase. In addition, the square particles in Fig. 3c and d are thought to indicate the transitional structure during the Ostwald ripening.

Fig. 5 shows the effects of holding time on volume fraction, V_f, of these undissolved $M_{23}C_6$ particles at 1373, 1423 and 1473 K. The volume fraction of the $M_{23}C_6$ particles steeply decreases with holding time in the beginning at each temperature, and then gradually decreases, approaching to the equilibrium state. Therefore, the structure is thought to reach quite near the equilibrium state after austenitizing for 240 s, which is enough time to stabilize the amount of the undissolved $M_{23}C_6$ particles at each temperature. The three SEM images (Fig. e, 3f and g), after austenitizing for 240 s, indicate the decrease in the amount of the undissolved $M_{23}C_6$ particles and their growth at higher temperature. Therefore, the dissolution and Ostwald ripening of $M_{23}C_6$ particles also proceed by heightening the austenitization temperature.

Table II lists the equilibrium chemical compositions of the γ phase at temperatures between 1273 and 1473 K calculated by Thermo-calc. Chromium and carbon concentration in γ phase increases with temperature, while that of nickel and aluminum decrease. This increase in chromium and carbon concentration is due to the dissolution of $M_{23}C_6$ particles into γ phase as mentioned above.

M_s and M_f temperatures determined by experiment are shown in Fig. 6, with M_s temperatures calculated from the chemical composition of γ phase listed in Table II using the following Equation 1.

$$M_s(\mathrm{K}) = 834 - 474\mathrm{x[mass\%C]} - 33\mathrm{x[mass\%Mn]} - 17\mathrm{x[mass\%Ni]} - 17\mathrm{x[mass\%Cr]} + 2\mathrm{x[mass\%Al]} - 7\mathrm{x[mass\%Si]} \quad (1)$$

TABLE II Equilibrium chemical compositions of the γ phase between 1273 and 1473 K calculated by Thermo-calc. (mass%)

Temperature (K)	C	Ni	Cr	Al	Fe
1273	0.15	2.53	13.24	0.69	Bal.
1323	0.20	2.48	13.76	0.68	Bal.
1348	0.24	2.46	14.04	0.67	Bal.
1373	0.27	2.45	14.35	0.65	Bal.
1398	0.31	2.45	14.77	0.61	Bal.
1423	0.35	2.44	15.00	0.60	Bal.
1473	0.44	2.41	15.47	0.57	Bal.

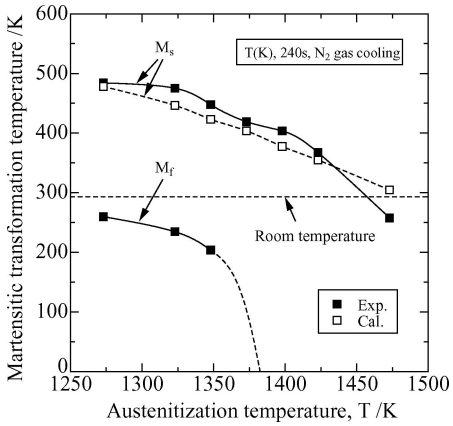

Figure 6 Effects of austenitization temperatures on martensite start (M_s) and finish (M_f) temperatures.

Equation 1 uses the data on the effects of C, Mn, Ni and Cr on M_s cited from the paper by Steven and Haynes [9], and the data of Al and Si by Ishida [10]. In this calculation, it was assumed that Mn and Si dissolved completely in γ matrix. The experimental M_s temperatures exhibit similar values to the calculated ones, and the experimental M_s and M_f temperatures decrease with increasing austenitization temperature. This decrease in M_s and M_f results in the change of the microstructures and XRD patterns of the matrix phase. In the annealed structure before austenitizing, some grains with about 3 μm in diameter are observed (Fig. 3a). On the other hand, the features of the matrix phase after austenitizing are quite different from that of the annealed one. That is, the surface of the matrix phase is uneven in the structure after austenitizing at 1373 K for 240 s (Fig. 3f), while large grains are clearly observed after austenitizing at 1423 and 1473 K for 240 s (Fig. 3e and g).

As for the XRD patterns, α phase is identified as a matrix phase in the annealed alloy (Fig. 4B(a)), while α', with broad peak compared with α, and retained γ phases (γ_R) appear in the alloys after austenitizing (Fig. 4B(b)–(g)). From three XRD patterns with different austenitization temperatures (f 1373 K, (e)1423 K and (g)1473 K) and same holding time(240 s), higher austenitization temperature tends to heighten the X-ray intensity of retained γ phase, and reduces the intensity of α' phase. In other words, the γ phase is stabilized due to the decrease in M_s

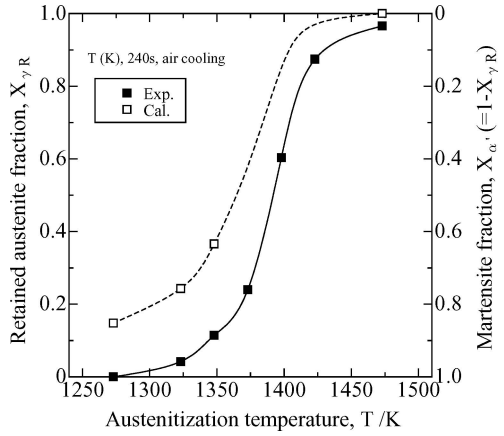

Figure 7 Effects of austenitization temperatures on retained austenite and martensite fraction.

and M_f at higher austenitization temperature. The grains with about 3 μm in diameter, uneven surface and the large clear grains in Fig. 3 are thought to be closely related to the α, α' and retained γ phases shown in Fig. 4B, respectively.

The double peaks detected near $2\theta = 100^\circ$ for the annealed alloy (Fig. 4B(a)) and near $2\theta = 90^\circ$ for the austenitized ones at 1423 and 1473 K for 240 s (Fig. 4B(e) and (g)) are thought to be the K_α double lines [6], which should exist in all samples. However, the other XRD patterns after austenitizing exhibit no clear double peaks (Fig. 4B(b), (c), (d) and (f)). These results are probably due to the broadening of their X-ray peaks because they have α' phase with much dislocation in the structures.

Fig. 7 shows the effect of austenitization temperature on retained austenite fraction, $X_{\gamma R}$, and martensite fraction, $X'_{\alpha'}$ (=1−$X_{\gamma R}$). The mark "■" in the figure indicates the experimental values measured by XRD. The experimental $X_{\gamma R}$ value increases with austenitization temperature, describing an s-shape curve. This tendency is opposite to the relation between magnetization and austenitization temperature shown in Fig. 1. Therefore, the high J value (1.46 T) of the annealed alloy is due to the ferromagnetic α matrix phase, and the decrease in J values at higher temperature is due to the increase in the paramagnetic retained austenite fraction in the microstructure. In addition, the decrease in J values with holding time (Fig. 2) is due to the same reason because the XRD intensity of retained γ phase also heightens when the holding time varies as shown in Fig. 4B(b)–(e).

On the other hand, the mark "□" in Fig. 7 indicates the calculated $X_{\gamma R}$ and $X_{\alpha'}$ values determined from the measured M_s and M_f temperatures in Fig. 6 using the following Equations 2 and 3.

$$X_{\gamma R}(\text{cal.}) = (R.T. - M_f)/(M_s - M_f) \quad (2)$$

$$X\alpha'(\text{cal.}) = (M_s - R.T.)/(M_s - M_f) \quad (3)$$

Where R.T. is equal to 293 K. These calculated $X_{\gamma R}$ (cal.) and $X_{\alpha'}$ (cal.) values could be determined at three austenitization temperatures of 1273, 1323 and 1348 K because both M_s and M_f are known at these temperatures. Unfortunately, these calculated values could not been determined at austenitization temperatures between 1373 and 1423 K because M_f temperatures are unknown in this range. However, at higher austenitization temperature of 1473 K, the $X_{\gamma R}$ (cal.) value should be equal to 1 because M_s is 257 K below the room temperature. Compared the experimental and calculated values, the $X_{\gamma R}$ (exp.) and $X_{\gamma R}$ (cal.) values respectively exhibit almost same values of 0.966 and 1 at high austenitization temperature of 1473 K. However, the $X_{\gamma R}$ (exp.) values are smaller than $X_{\gamma R}$ (cal.), in other words, the $X_{\alpha'}$ (exp.) values are high compared with $X_{\alpha'}$ (cal.) at lower austenitization temperatures between 1273 and 1348 K.

Once part of the γ phaseis transformed into α' structure, the elastic strain is generated in γ matrix phase near the α'/γ interface because of the volume expansion in $\gamma \rightarrow \alpha'$ transformation, and large driving force is required for further $\gamma \rightarrow \alpha'$ transformation in the later stage of the transformation compared with that in the earlier stage [11]. In other words, the required driving force for $\gamma \rightarrow \alpha'$ transformation should be relatively small in the earlier stage just below the M_s compared with that in the later stage. However, the Equations 2 and 3 take no thought of this change in driving force during $\gamma \rightarrow \alpha'$ transformation, and presuppose the constant driving force from M_s to M_f. It is considered that the actual driving force is probably lower than the presupposed constant driving force in the earlier stage of the $\gamma \rightarrow \alpha'$ transformation. Therefore, the $X_{\alpha'}$ (exp.) exhibits higher values than $X_{\alpha'}$ (cal.), and the change of the driving force during $\gamma \rightarrow \alpha'$ transformation should be also considered in order to predict exact $X_{\gamma R}$ and $X_{\alpha'}$ values from M_s and M_f temperatures.

Fig. 8 shows the relation between retained austenite fraction, $X_{\gamma R}$, and J values obtained from Figs 1 and 7.

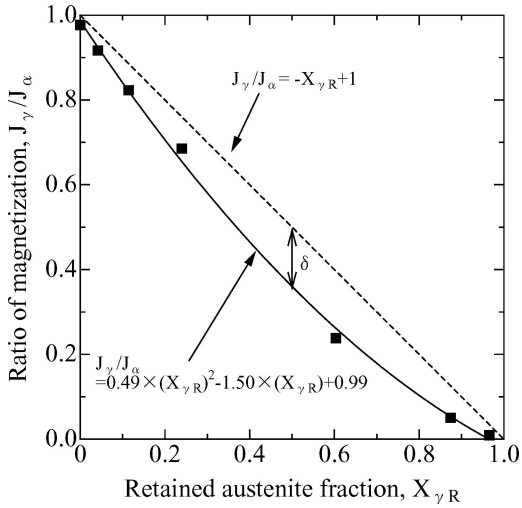

Figure 8 Relation between magnetization and retained austenite fraction.

Their relation is approximately expressed as the following equation 4, where J_γ means the J values of the alloy after austenitizing at temperatures between 1273 and 1473 K, while J_α means that of the alloy after annealing at 1053 K (=1.46 T).

$$J_\gamma / J_\alpha = 0.49X_{\gamma R}^2 - 1.50X_{\gamma R} + 0.99 \quad (4)$$

It should be noted that their relation is not expressed as a simple linear function, $J_\gamma/J_\alpha = -X_{\gamma R}+1$, drawn as a broken line in Fig. 8. The deviation, δ, from the linear function is expressed as the following Equation 5.

$$\begin{aligned}\delta &= \left(-X_{\gamma R} + 1\right) - \left(0.49X_{\gamma R}^2 - 1.50X_{\gamma R} + 0.99\right) \\ &= -0.49\left(X_{\gamma R} - 0.51\right)^2 + 0.13 \quad (5)\end{aligned}$$

From Equation 5, the δ exhibits the maximum value when $X_{\gamma R}$ is nearly equal to 0.5, that is, about 50% of α' and 50% of retained γ phases are mixed in the structure. As mentioned above, the elastic strain is introduced near the α'/γ interface. Especially when 50% of α' and 50% of γ_R are mixed in the structure, the total amount of the elastic strain probably exhibits the maximum value because the most amount of α'/γ interface should exist in the structure. Therefore, it is also considered that the amount of the elastic strain near the α'/γ interface is closely related to the deviation from the linear law in Fig. 8. In addition, not only the retained austenite fraction but also the chemical composition of the matrix phases, the grain size, the amount and the size of the carbide particles vary with austenitization temperature and holding time as shown in Table II and Fig. 3. In general, the increase in chromium and carbon content with increasing austenitization temperature and holding time tends to reduce the magnetization. On the other hand, the decrease in nickel and aluminum content tends to heighten the magnetization. Furthermore, the grain growth and the decrease in the amount of the fine carbide particles at higher temperature for longer holding time tend to make the domain wall motion easy, and raise the magnetization. Thus, it is considered that the complex effects of elastic strain near α'/γ interface, chemical composition, grain size and distribution of the carbide particles on magnetization cause the deviation from the simple linear law in Fig. 8.

4. Conclusion

(1). Fe-17.5 mass%Cr-2.0 mass%Ni-0.8 mass%Al-0.5 mass%C based alloy exhibited high magnetization of $J = 1.46$ T after annealing at 1053 K. On the other hand, the J values of the alloy after austenitizing at temperatures between 1273 and 1473 K lowered with increasing austenitization temperature, describing s-shape curves. The J value of the alloy after austenitizing at temperatures above 1423 K for 240 s was nearly equal to zero magnetization. In addition, the J values also lowered with the increase of the holding time between 1 s and 240 s.

(2). The decrease in J values by austenitizing at higher temperatures for longer time was closely related to the dissolution of the $M_{23}C_6$ particles into γ matrix phase, which proceeds at higher temperature for longer time. The increase in chromium and carbon concentration in γ matrix due to the dissolution of $M_{23}C_6$ particles resulted in the decrease in M_s and M_f temperature, and stabilized the retained γ structure. The increase in the amount of the paramagnetic retained γ phase reduced the J values.

(3). The following equation was introduced on the relation between retained austenite fraction, $X_{\gamma R}$, and magnetization, J (T).

$$J_\gamma / J_\alpha = 0.49X_{\gamma R}^2 - 1.50_{\gamma R} + 0.99$$

J_γ means the J values of the alloy after austenitizing at temperatures between 1273 and 1473 K, while $J_\alpha$means that of the alloy after annealing at 1053 K (=1.46 T). The deviation, δ, from a simple linear function, $J_\gamma/J_\alpha = -X_{\gamma R}+1$, exhibits the maximum value when $X_{\gamma R}$ value is nearly equal to 0.5. It was suggested that the complex effects of elastic strain near α'/γ interface, chemical composition, grain size and distribution of the carbide particles on magnetization cause the deviation from the simple linear function.

Acknowledgment

The authors would like to thank to Dr. Rikizo Watanabe, the former general manager of the Metallurgical Research Laboratory, Hitachi Metals, for giving us some beneficial advices in writing this paper.

References

1. "Binary alloy phase diagrams", edited by T. B. Massalski (American Society for Metals, Metals Park, Ohio, 1986) pp. 112, 562, 822, 1086.
2. S. YOKOYAMA and T. INUI, *Tetsu-to-Hagane* **88** (2002) 222.
3. S. YOKOYAMA, T. INUI and Y. MINAMINO, *J. Mater. Sci.* **38** (2003) 4535.
4. S. YOKOYAMA, T. INUI, Y. MINAMINO and N. TSUJI, *Tetsu-to-Hagane* **89** (2003) 803.
5. S. YOKOYAMA and H. SASAKI, *Hitachi Met. Techn. Rev.* **19** (2003) 57.
6. B. D. CULLITY, "Elements of X-Ray Diffraction", 2nd ed. (translated into Japanese by G. Matsumura), AGNE, Tokyo (1980) pp. 8, 374.
7. K. KUO, *J. Iron Steel Inst.* **173** (1953) 363.
8. K. BUNGARDT, E. KUNZE and E. HORN, *Arch. Eisenhüttenwes.* **29** (1958) 193.
9. W. STEVEN and A. G. HAYNES, *J. Iron Steel Inst.* **183** (1956) 349.
10. K. ISHIDA, *J. Alloys and Compounds* **220** (1995) 126.
11. K. SUGIMOTO, K. OSAMURA, T. YAMANE, M. MAKI, S. KIKUCHI, S. OCHIAI and Y. MURAKAMI, "Metallography", (in Japanese), Asakurasyoten, Tokyo (1991) 125.

Received 29 November 2004
and accepted 27 May 2005